






Article

Darcy–Forchheimer MHD Couple Stress 3D Nanofluid over an Exponentially Stretching Sheet through Cattaneo–Christov Convective Heat Flux with Zero Nanoparticles Mass Flux Conditions

Muhammad Wakeel Ahmad ¹, Poom Kumam ^{2,3,4,*} , Zahir Shah ^{2,5,*} , Ali Ahmad Farooq ⁶, Rashid Nawaz ¹ , Abdullah Dawar ⁷ , Saeed Islam ¹  and Phatiphat Thounthong ⁸

¹ Department of Mathematics, Abdul Wali Khan University, Mardan 23200, Pakistan

² KMUTT-Fixed Point Research Laboratory, Room SCL 802 Fixed Point Laboratory, Science Laboratory Building, Department of Mathematics, Faculty of Science, King Mongkut's University of Technology Thonburi (KMUTT), 126 Pracha-Uthit Road, Bang Mod, Thrung Khru, Bangkok 10140, Thailand

³ KMUTT-Fixed Point Theory and Applications Research Group, Theoretical and Computational Science Center (TaCS), Science Laboratory Building, Faculty of Science, King Mongkut's University of Technology Thonburi (KMUTT), 126 Pracha-Uthit Road, Bang Mod, Thrung Khru, Bangkok 10140, Thailand

⁴ Department of Medical Research, China Medical University Hospital, China Medical University, Taichung 40402, Taiwan

⁵ Center of Excellence in Theoretical and Computational Science (TaCS-CoE), SCL 802 Fixed Point Laboratory, Science Laboratory Building, King Mongkut's University of Technology Thonburi (KMUTT), 126 Pracha-Uthit Road, Bang Mod, Thrung Khru, Bangkok 10140, Thailand

⁶ Mathematics Department, COMSATS University, Abbottabad Campus, Islamabad 22060, Pakistan

⁷ Department of Mathematics, Qurtuba University of Science and Information Technology, Peshawar 25000, Pakistan

⁸ Renewable Energy Research Centre, Department of Teacher Training in Electrical Engineering, Faculty of Technical Education, King Mongkut's University of Technology North Bangkok, 1518 Pracharat 1 Road, Bangsue, Bangkok 10800, Thailand

* Correspondence: poom.kum@kmutt.ac.th (P.K.); zahir.sha@kmutt.ac.th (Z.S.); Tel.: +66-2-4708-994 (P.K. & Z.S.)

Received: 17 June 2019; Accepted: 5 August 2019; Published: 6 September 2019



Abstract: In the last decade, nanoparticles have provided numerous challenges in the field of science. The nanoparticles suspended in various base fluids can transform the flow of fluids and heat transfer characteristics. In this research work, the mathematical model is offered to present the 3D magnetohydrodynamics Darcy–Forchheimer couple stress nanofluid flow over an exponentially stretching sheet. Joule heating and viscous dissipation impacts are also discussed in this mathematical model. To examine the relaxation properties, the proposed model of Cattaneo–Christov is supposed. For the first time, the influence of temperature exponent is scrutinized via this research article. The designed system of partial differential equations (PDE's) is transformed to set of ordinary differential equations (ODE's) by using similarity transformations. The problem is solved analytically via homotopy analysis technique. Effects of dimensionless couple stress, magnetic field, ratio of rates, porosity, and coefficient of inertia parameters on the fluid flow in x - and y -directions have been examined in this work. The augmented ratio of rates parameter upsurses the velocity profile in the x -direction. The augmented magnetic field, porosity parameter, coefficient of inertia, and couple stress parameter diminishes the velocity field along the x -direction. The augmented magnetic field, porosity parameter, coefficient of inertia, ratio of rates parameter, and couple stress parameter reduces the velocity field along the y -axis. The influences of time relaxation, Prandtl number, and temperature exponent on temperature profile are also discussed. Additionally, the influences of thermophoresis parameter, Schmidt number, Brownian motion parameter, and temperature exponent

on fluid concentration are explained in this work. For engineering interests, the impacts of parameters on skin friction and Nusselt number are accessible through tables.

Keywords: MHD; nanofluids; heat transfer; couple stress fluid; HAM; Cattaneo–Christov heat flux model

1. Introduction

Nanofluids are used inside hybrid-powered machines, fuel cells, microelectronics, pharmaceutical procedures, and nanotechnologies. Choi [1] immersed nanoparticles into a base fluid for the first time. Wang and Mujumdar [2] prepared nanofluids by adding metallic and non-metallic nano-particles into base fluids and explained the heat transfer characteristics of the nanofluids. The study of Wang and Mujumdar was later numerically deliberated by Eastman et al. [3,4]. Tiwari and Das [5] designed a model for single-phase nanofluids, but, in contrast, Buongiorno [6] constructed the second-phase mathematical model for nanofluids. Soon after, numerous researchers have been conducted in diverse regions of interest regarding nanofluids. Kasaeian et al. [7] worked on the performance of heat transmission in nanofluid flow. Ramzan et al. [8] explored the radiative magnetohydrodynamic (MHD) flow of nanofluid. Sheikholeslami et al. [9] solved numerically the MHD nanofluid flow through a porous medium. Besthapu et al. [10] probed nanofluid mixed convection flow with MHD by observing the viscous dissipation impacts. Dawar et al. [11] scrutinized nanofluid flow over an unsteady oscillatory stretching sheet. Alharbi et al. [12] included the MHD effects and examined the entropy generation. Shah et al. [13] probed Darcy–Forchheimer nanofluid flow with inertial effect. Khan et al. [14] studied MHD flow of Darcy–Forchheimer nanofluid with the impact of thermal radiation. Zubair et al. [15] explored 3D Darcy–Forchheimer squeezing nanofluid flow with Cattaneo–Christov heat flux via entropy generation. Khan et al. [16] studied the flow of nanofluid past a linearly stretching surface. The MHD nanofluid flow via entropy generation with viscous dissipation impact was explored by Dawar et al. [17]. Sheikholeslami [18] explored free convective nanofluid in medium under effect of electric field. Sheikholeslami [19] investigated the flow of water-based nanofluid with Brownian motion magnetic field impacts. Dawar et al. [20] explored Darcy–Forchheimer flow of nanofluids over stretching surface analytically via convective conditions. Ramzan et al. [21] examined the heat transfer rate in couple stress MHD nanofluid flow.

In 1822, Fourier [22] designed a heat transmission model for the material. Later on, Cattaneo [23] modified the Fourier model by adding a term of thermal relaxation time. Afterwards Christov [24] further improved the Cattaneo model [23], called the Cattaneo–Christov heat flux model. Straughan [25] deliberated the stability of wave motion in a porous medium by applying the Cattaneo–Christov heat flux model. Straughan [26] investigated the characteristics of heat transmission in a nanofluid. Han et al. [27] explicated the thermal transmission in viscoelastic fluids. Khan et al. [28] numerically calculated [24] over an exponentially stretching surface. Hayat et al. [29] deliberated various features of advanced mass and the heat flux model of the nanofluid flow. Tibullo et al. [30] probed the model of [24] for incompressible fluids. Ciarletta et al. [31] constructed a stability and uniqueness model for [24]. Haddad [32] examined thermal stability for model [24] in porous medium. Mustafa [33] took model [24] and explained it for heat transfer in a rotating flow of nanofluid. Hayat et al. [34] investigated impacts of model [24] during the flow of various fluids. Waqas et al. [35] assumed Burger’s fluids thermal conductivity by taking model [24]. Zheng et al. [36] investigated the viscoelastic MHD fluid flow and heat transmission past a stretching sheet by applying model [24]. Shah et al. [37] explored MHD flow of an electrically-conducting ferrofluid by taking model [24] over a stretching surface. Hayat et al. [38] took model [24] and probed 3D nanofluid flow over a stretching surface. Muskat et al. [39] explained the nature of homogeneous fluid flow through a porous medium. Seddeek et al. [40] assumed the Darcy–Forchheimer model and studied the flow of mixed convention fluid

with the effects of viscous dissipation and thermophoresis. Pal et al. [41] explored the nature of fluid flow in a porous medium by taking Darcy–Forchheimer model. Sadiq et al. [42] explored the MHD flow of the Maxwell nanofluid through a heated sheet by assuming the Darcy–Forchheimer model. Wakif et al. [43] numerically examined the nanofluid flow with external magnetic field. Wakif et al. [44] examined the MHD nanofluid flow with thermal radiation impact. Wakif et al. [45] scrutinized the water-based nanofluid with uniform magnetic field impact. The other related studies of Wakif et al. can be seen in [46–49]. Zubiar et al. [50] studied entropy generation in a squeezing nanofluid flow.

The main aim of this investigation is to study the 3D magnetohydrodynamic flow of Darcy–Forchheimer couple stress nanofluid over a porous exponentially stretching film. The present work is done with joule heating and viscous dissipation effects. To examine the thermal relaxation time, the Cattaneo–Christov model of heat flux is applied. For the first time, the influences of the temperature exponent are explored through this research article.

2. Problem Formulation

Assume 3D couple stress nanofluids flow over a porous exponentially stretching sheet, having null mass flux and convection of heat conditions. Stretching velocity in the x -direction is of the form $u = U_w(x, y) = U_0 e^{\frac{x+y}{L}}$, while velocity in the y -direction is to be assumed as $v = V_w(x, y) = V_0 e^{\frac{x+y}{L}}$, here (U_0, V_0) are constants (Figure 1). The joule heating, viscous dissipation, and impacts of uniform magnetic field are applied in the present nanofluids flow model. A uniform magnetic field is assumed in the z -direction. The temperature of the porous stretching surface will be kept at continual temperature T_w , while surroundings temperature is T_∞ , constant concentration denoted by C_w and C_∞ shows ambient concentration.

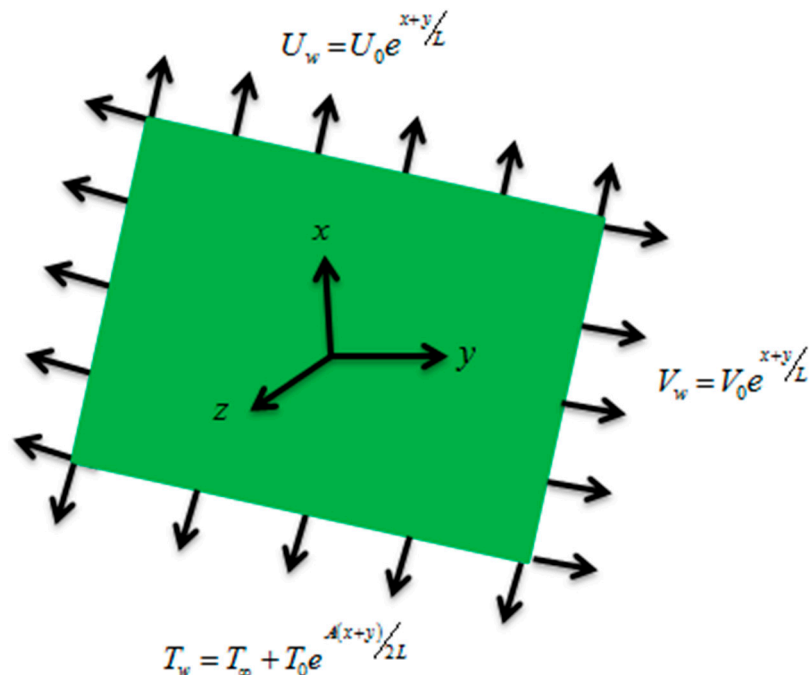


Figure 1. Geometrical representation of the flow.

The governing equations of the modeled problem are [21,38]:

$$\frac{\partial u}{\partial x} + \frac{\partial v}{\partial y} + \frac{\partial w}{\partial z} = 0, \tag{1}$$

$$u \frac{\partial u}{\partial x} + v \frac{\partial u}{\partial y} + w \frac{\partial u}{\partial z} = \nu \frac{\partial^2 u}{\partial z^2} - \nu' \frac{\partial^4 u}{\partial z^4} - \frac{\sigma B_0^2}{\rho} u - \left(\frac{\nu}{k} + Fu \right) u, \tag{2}$$

$$u \frac{\partial v}{\partial x} + v \frac{\partial v}{\partial y} + w \frac{\partial v}{\partial z} = v \frac{\partial^2 v}{\partial z^2} - \nu' \frac{\partial^4 v}{\partial z^4} - \frac{\sigma B_0^2}{\rho} v - \left(\frac{\nu}{k} + Fv \right) v, \quad (3)$$

$$\rho c_p \left(u \frac{\partial T}{\partial x} + v \frac{\partial T}{\partial y} + w \frac{\partial T}{\partial z} \right) = -\nabla \cdot \vec{q}, \quad (4)$$

$$u \frac{\partial C}{\partial x} + v \frac{\partial C}{\partial y} + w \frac{\partial C}{\partial z} = D_B \left(\frac{\partial^2 C}{\partial z^2} \right) + \frac{D_T}{T_\infty} \left(\frac{\partial^2 T}{\partial z^2} \right), \quad (5)$$

The heat flux \vec{q} satisfies

$$\vec{q} + \lambda_e \left(\frac{\partial \vec{q}}{\partial t} + \vec{V} \cdot \nabla \vec{q} - \vec{q} \cdot \nabla \vec{V} + (\nabla \cdot \vec{V}) \vec{q} \right) = -\lambda_1 \nabla T, \quad (6)$$

where λ_e and λ_1 signify the thermal relaxation time and thermal conductivity, respectively. By taking $\lambda_e = 0$, Equation (6) reduced to Fourier's law. Furthermore eliminating \vec{q} from Equations (4) and (6), we obtained heat equation as under:

$$u \frac{\partial T}{\partial x} + v \frac{\partial T}{\partial y} + w \frac{\partial T}{\partial z} = \frac{\lambda_1}{\rho c_p} \left(\frac{\partial^2 T}{\partial z^2} \right) - \lambda_e \left[u^2 \frac{\partial^2 T}{\partial x^2} + v^2 \frac{\partial^2 T}{\partial y^2} + w^2 \frac{\partial^2 T}{\partial z^2} + 2uv \frac{\partial^2 T}{\partial x \partial y} + 2vw \frac{\partial^2 T}{\partial y \partial z} + 2uw \frac{\partial^2 T}{\partial x \partial z} + \left(u \frac{\partial u}{\partial x} + v \frac{\partial u}{\partial y} + w \frac{\partial u}{\partial z} \right) \frac{\partial T}{\partial x} + \left(u \frac{\partial v}{\partial x} + v \frac{\partial v}{\partial y} + w \frac{\partial v}{\partial z} \right) \frac{\partial T}{\partial y} + \left(u \frac{\partial w}{\partial x} + v \frac{\partial w}{\partial y} + w \frac{\partial w}{\partial z} \right) \frac{\partial T}{\partial z} \right], \quad (7)$$

with boundary conditions

$$u = U_w(x, y) = U_0 e^{\frac{x+y}{L}}, \quad v = V_w(x, y) = V_0 e^{\frac{x+y}{L}}, \quad w = 0, \quad k \frac{\partial T}{\partial z} = -h_f (T_w - T), \\ D_B \frac{\partial C}{\partial z} + \frac{D_T}{T_\infty} \frac{\partial T}{\partial x} = 0, \quad \text{at } z = 0, \\ u \rightarrow 0, \quad v \rightarrow 0, \quad C \rightarrow C_\infty, \quad T \rightarrow T_\infty \quad \text{as } z \rightarrow \infty. \quad (8)$$

The exceeding equations have velocity components u , v , w along their respective directions, ν shows kinematic viscosity, k indicates thermal conductivity, $F = C_b / \sqrt{Bx}$ is the inertial coefficient of permeable medium, $\nu' = \frac{\mu}{\rho}$ is the couple stress viscosity, where n defines viscosity parameter, σ is the electric charge density, ρ is the density, h_f is the heat transfer coefficient, A is the temperature exponent, C_p indicates specific heat, D_B is the Brownian diffusion coefficient, D_T is the thermophoresis diffusion coefficient, and L is the reference length.

Applying the following similarity transformations techniques [21]

$$u = U_0 e^{\frac{x+y}{L}} f', \quad v = U_0 e^{\frac{x+y}{L}} g', \quad w = -\left(\frac{\nu U_0}{2L} \right)^{\frac{1}{2}} e^{\frac{x+y}{2L}} (f + \xi f' + g + \xi g'), \\ T_w = T_\infty + T_0 e^{\frac{A(x+y)}{2L}} \theta, \quad C_w = C_\infty + C_0 e^{\frac{A(x+y)}{2L}} \phi, \quad \xi = \left(\frac{U_0}{2\nu L} \right)^{\frac{1}{2}} e^{\frac{x+y}{2L}} z. \quad (9)$$

Equation (1) is gratified inexorably, and Equations (2)–(7) yield

$$f''' - 2(f' + g')f' + (f + g)f'' - Kf^v - (M^2 + \kappa + Frf')f' = 0, \quad (10)$$

$$g''' - 2(f' + g')g' + (f + g)g'' - Kg^v - (M^2 + \kappa + Frg')g' = 0, \quad (11)$$

$$\frac{1}{Pr} \theta'' - A(f' + g')\theta + (f + g)\theta' + \frac{\Lambda}{2} \left[\left\{ \xi(f' + g') + (1 + 2A)(f + g) \right\} (f' + g')\theta' - A \left\{ (A + 2)(f' + g')^2 - (f + g)(f'' + g'') \right\} \theta - (f + g)^2 \theta'' \right] = 0, \quad (12)$$

$$\phi'' - ScA(f' + g')\phi + Sc(f + g)\phi' + \frac{Nt}{Nb} \theta'' = 0, \quad (13)$$

Satisfying the following boundary conditions

$$\begin{aligned} f = 0, \quad f' = 1, \quad g = 0, \quad g' = \alpha, \quad \theta' = -\gamma(1 - \theta), \quad Nb\phi' + Nt\theta' = 0 \quad \text{at } \xi = 0, \\ f' \rightarrow 0, \quad g' \rightarrow 0, \quad \theta \rightarrow 0, \quad \phi \rightarrow 0 \quad \text{as } \xi \rightarrow \infty. \end{aligned} \quad (14)$$

In Equations (9)–(13), $K = \frac{\nu'a}{\nu^2}$ indicates dimensionless couple stress parameter, $M^2 = \frac{2\sigma B_0^2 L}{\rho U_w}$ represents the Hartmann number, $\alpha = \frac{V_0}{U_0}$ indicates the quotient of rates parameter, $\kappa = \frac{2\nu L}{k U_w}$ indicates the porosity parameter, $Fr = \frac{2\nu C_b}{\sqrt{B_x}}$ indicates the coefficient of inertia, $Pr = \frac{\nu \rho c_p}{\lambda_1}$ represents the Prandtl number, $\Lambda = \frac{\lambda_e U_w}{L}$ represents dimensionless thermal relaxation time, $Sc = \frac{\nu}{D_B}$ represents Schmidt number, $\gamma = \frac{h}{k} \sqrt{\frac{2\nu L}{U_w}}$ indicates the Biot number, $Nb = \frac{\tau D_B}{\nu} (C_w - C_\infty)$ represents the Brownian motion parameter, and $Nt = \frac{\tau D_T (T_w - T_\infty)}{\nu T_\infty}$ represents thermophoresis parameter.

$$\begin{aligned} C_{fx} \sqrt{\left(\frac{Re_x}{2}\right)} &= e^{\frac{3(x+y)}{2L}} f''(0), \\ C_{fy} \sqrt{\left(\frac{Re_x}{2}\right)} &= e^{\frac{3(x+y)}{2L}} g''(0), \end{aligned} \quad (15)$$

3. Solution by HAM

Homotopy Analysis method (HAM) is applied to solve Equations (10)–(13) with boundary condition (14).

The initial guesses are assumed as:

$$f_0(\xi) = 1 - e^{-\xi}, \quad g_0(\xi) = \alpha(1 - e^{-\xi}), \quad \theta_0(\xi) = \left(\frac{\gamma}{\gamma + 1}\right)e^{-\xi}, \quad \phi_0(\xi) = -\left(\frac{Nt}{Nb} \frac{\gamma}{\gamma + 1}\right)e^{-\xi}. \quad (16)$$

$L_f, L_g, L_\theta,$ and L_ϕ are selected as:

$$L_f(f) = f''' - f', \quad L_g(g) = g''' - g', \quad L_\theta(\theta) = \theta'' - \theta, \quad L_\phi(\phi) = \phi'' - \phi, \quad (17)$$

with the following resultant characteristics:

$$\begin{aligned} L_f(k_1 + k_2 e^{-\xi} + k_3 e^\xi) &= 0, \quad L_g(k_4 + k_5 e^{-\xi} + k_6 e^\xi) = 0, \\ L_\theta(k_7 e^{-\xi} + k_8 e^\xi) &= 0, \quad L_\phi(k_9 e^{-\xi} + k_{10} e^\xi) = 0, \end{aligned} \quad (18)$$

Here $k_i (i = 1, 2, 3, \dots, 10)$ represents real constants in general solution of the modeled problem.

The consequential non-linear operators N_f, N_g, N_θ and N_ϕ are specified as under:

$$\begin{aligned} N_f[f(\xi; \mathfrak{R}), g(\xi; \mathfrak{R})] &= \frac{d^3 f(\xi; \mathfrak{R})}{d\xi^3} - 2\left(\frac{df(\xi; \mathfrak{R})}{d\xi} + \frac{dg(\xi; \mathfrak{R})}{d\xi}\right) \frac{df(\xi; \mathfrak{R})}{d\xi} \\ &+ (f(\xi; \mathfrak{R}) + g(\xi; \mathfrak{R})) \frac{d^2 f(\xi; \mathfrak{R})}{d\xi^2} - K \frac{d^5 f(\xi; \mathfrak{R})}{d\xi^5} - \left\{M^2 + \kappa + Fr \frac{df(\xi; \mathfrak{R})}{d\xi}\right\} \frac{df(\xi; \mathfrak{R})}{d\xi}, \end{aligned} \quad (19)$$

$$\begin{aligned} N_g[g(\xi; \mathfrak{R}), f(\xi; \mathfrak{R})] &= \frac{d^3 g(\xi; \mathfrak{R})}{d\xi^3} - 2\left(\frac{df(\xi; \mathfrak{R})}{d\xi} + \frac{dg(\xi; \mathfrak{R})}{d\xi}\right) \frac{dg(\xi; \mathfrak{R})}{d\xi} \\ &+ (f(\xi; \mathfrak{R}) + g(\xi; \mathfrak{R})) \frac{d^2 g(\xi; \mathfrak{R})}{d\xi^2} - K \frac{d^5 g(\xi; \mathfrak{R})}{d\xi^5} - \left\{M^2 + \kappa + Fr \frac{dg(\xi; \mathfrak{R})}{d\xi}\right\} \frac{dg(\xi; \mathfrak{R})}{d\xi}, \end{aligned} \quad (20)$$

$$\begin{aligned}
 N_\theta[\theta(\xi; \mathfrak{R}), f(\xi; \tau), g(\xi; \mathfrak{R})] &= \frac{1}{\text{Pr}} \frac{d^2\theta(\xi; \mathfrak{R})}{d\xi^2} - A \left(\frac{df(\xi; \mathfrak{R})}{d\xi} + \frac{dg(\xi; \mathfrak{R})}{d\xi} \right) \theta(\xi; \mathfrak{R}) \\
 &+ (f(\xi; \mathfrak{R}) + g(\xi; \mathfrak{R})) \frac{d\theta(\xi; \mathfrak{R})}{d\xi} + \frac{\Lambda}{2} \left\{ \begin{aligned} &\xi \left(\frac{df(\xi; \mathfrak{R})}{d\xi} + \frac{dg(\xi; \mathfrak{R})}{d\xi} \right) \\ &+ (1 + 2A) \left(\begin{aligned} &f(\xi; \mathfrak{R}) \\ &+ g(\xi; \mathfrak{R}) \end{aligned} \right) \end{aligned} \right\} \left(\begin{aligned} &\frac{df(\xi; \mathfrak{R})}{d\xi} \\ &+ \frac{dg(\xi; \mathfrak{R})}{d\xi} \end{aligned} \right) \frac{d\theta(\xi; \mathfrak{R})}{d\xi} \\
 &- A \left\{ (A + 2) \left(\frac{df(\xi; \mathfrak{R})}{d\xi} + \frac{dg(\xi; \mathfrak{R})}{d\xi} \right)^2 - \left(\begin{aligned} &f(\xi; \mathfrak{R}) \\ &+ g(\xi; \mathfrak{R}) \end{aligned} \right) \left(\frac{d^2f(\xi; \mathfrak{R})}{d\xi^2} + \frac{d^2g(\xi; \mathfrak{R})}{d\xi^2} \right) \right\} \theta(\xi; \mathfrak{R}) \\
 &- (f(\xi; \mathfrak{R}) + g(\xi; \mathfrak{R}))^2 \frac{d^2\theta(\xi; \mathfrak{R})}{d\xi^2} \Big], \tag{21}
 \end{aligned}$$

$$\begin{aligned}
 N_\Phi[\Phi(\xi; \mathfrak{R}), f(\xi; \mathfrak{R}), g(\xi; \mathfrak{R}), \theta(\xi; \mathfrak{R})] &= \frac{d^2\Phi(\xi; \mathfrak{R})}{d\xi^2} - \\
 \text{ScA} \left(\frac{df(\xi; \mathfrak{R})}{d\xi} + \frac{dg(\xi; \mathfrak{R})}{d\xi} \right) \Phi(\xi; \mathfrak{R}) &+ \text{Sc} \cdot (f(\xi; \mathfrak{R}) + g(\xi; \mathfrak{R})) \frac{d\Phi(\xi; \mathfrak{R})}{d\xi} + \frac{Nt}{Nb} \frac{d^2\theta(\xi; \mathfrak{R})}{d\xi^2}, \tag{22}
 \end{aligned}$$

The zeroth-order problems from Equations (9)–(15) are:

$$(1 - \mathfrak{R})L_f[f(\xi; \mathfrak{R}) - f_0(\xi)] = \mathfrak{R}\hbar_f N_f[f(\xi; \mathfrak{R}), g(\xi; \mathfrak{R})], \tag{23}$$

$$(1 - \mathfrak{R})L_g[g(\xi; \mathfrak{R}) - g_0(\xi)] = \mathfrak{R}\hbar_g N_g[g(\xi; \mathfrak{R}), f(\xi; \mathfrak{R})], \tag{24}$$

$$(1 - \mathfrak{R})L_\theta[\theta(\xi; \mathfrak{R}) - \theta_0(\xi)] = \mathfrak{R}\hbar_\theta N_\theta[\theta(\xi; \mathfrak{R}), f(\xi; \mathfrak{R}), g(\xi; \mathfrak{R})], \tag{25}$$

$$(1 - \mathfrak{R})L_\Phi[\Phi_p(\xi; \mathfrak{R}) - \Phi_0(\xi)] = \mathfrak{R}\hbar_\Phi N_\Phi[\Phi(\xi; \mathfrak{R}), f(\xi; \mathfrak{R}), g(\xi; \mathfrak{R}), \theta(\xi; \mathfrak{R})], \tag{26}$$

The equivalent boundary conditions are:

$$\begin{aligned}
 f(\xi; \mathfrak{R})|_{\xi=0} = 0 & \quad \frac{df(\xi; \mathfrak{R})}{d\xi}|_{\xi=0} = 1 & \quad \frac{df(\xi; \mathfrak{R})}{d\xi}|_{\xi \rightarrow \infty} = 0 \\
 g(\xi; \mathfrak{R})|_{\xi=0} = 0 & \quad \frac{dg(\xi; \mathfrak{R})}{d\xi}|_{\xi=0} = \alpha & \quad \frac{dg(\xi; \mathfrak{R})}{d\xi}|_{\xi \rightarrow \infty} = 0 \\
 \theta(\xi; \mathfrak{R})|_{\xi \rightarrow \infty} = 0 & \quad \frac{d\theta(\xi; \mathfrak{R})}{d\xi}|_{\xi=0} = -\gamma(1 - \theta(\xi; \mathfrak{R})) \\
 \Phi(\xi; \mathfrak{R})|_{\xi \rightarrow \infty} = 0 & \quad Nb \frac{d\Phi(\xi; \mathfrak{R})}{d\xi}|_{\xi=0} = -Nt \frac{d\theta(\xi; \mathfrak{R})}{d\xi}|_{\xi=0}
 \end{aligned} \tag{27}$$

When $\mathfrak{R} = 0$ and $\mathfrak{R} = 1$ we have:

$$\begin{aligned}
 f(\xi; 0) = f_0(\xi), \quad f(\xi; 1) = f(\xi), \\
 g(\xi; 0) = g_0(\xi), \quad g(\xi; 1) = g(\xi), \\
 \theta(\xi; 0) = \theta_0(\xi), \quad \theta(\xi; 1) = \theta(\xi), \\
 \Phi(\xi; 0) = \Phi_0(\xi), \quad \Phi(\xi; 1) = \Phi(\xi).
 \end{aligned} \tag{28}$$

By Taylor’s series expansion $f(\xi; \mathfrak{R}), g(\xi; \mathfrak{R}), \theta(\xi; \mathfrak{R})$ and $\phi(\xi; \mathfrak{R})$ can be written as:

$$\begin{aligned}
 f(\xi; \mathfrak{R}) = f_0(\xi) + \sum_{q=1}^{\infty} f_q(\xi) \mathfrak{R}^q, \quad g(\xi; \mathfrak{R}) = g_0(\xi) + \sum_{q=1}^{\infty} g_q(\xi) \mathfrak{R}^q, \\
 \theta(\xi; \mathfrak{R}) = \theta_0(\xi) + \sum_{q=1}^{\infty} \theta_q(\xi) \mathfrak{R}^q, \quad \Phi(\xi; \mathfrak{R}) = \Phi_0(\xi) + \sum_{q=1}^{\infty} \Phi_q(\xi) \mathfrak{R}^q.
 \end{aligned} \tag{29}$$

where

$$\begin{aligned}
 f_q(\xi) = \frac{1}{q!} \frac{df(\xi; \mathfrak{R})}{d\xi} \Big|_{\mathfrak{R}=0}, \quad g_q(\xi) = \frac{1}{q!} \frac{dg(\xi; \mathfrak{R})}{d\xi} \Big|_{\mathfrak{R}=0}, \\
 \theta_q(\xi) = \frac{1}{q!} \frac{d\theta(\xi; \mathfrak{R})}{d\xi} \Big|_{\mathfrak{R}=0} \quad \text{and} \quad \Phi_q(\xi) = \frac{1}{q!} \frac{d\Phi(\xi; \mathfrak{R})}{d\xi} \Big|_{\mathfrak{R}=0}.
 \end{aligned} \tag{30}$$

The secondary constraints $\hbar_f, \hbar_g, \hbar_\theta$ and \hbar_Φ are chosen in such a way that the series in (29) becomes a convergent series at $\Re = 1$, by changing $\Re = 1$ in (29), we get:

$$\begin{aligned} f(\xi) &= f_0(\xi) + \sum_{q=1}^{\infty} f_q(\xi), \quad g(\xi) = g_0(\xi) + \sum_{q=1}^{\infty} g_q(\xi), \\ \theta(\xi) &= \theta_0(\xi) + \sum_{q=1}^{\infty} \theta_q(\xi), \quad \Phi(\xi) = \Phi_0(\xi) + \sum_{q=1}^{\infty} \Phi_q(\xi). \end{aligned} \tag{31}$$

For q^{th} – order solution of the problem:

$$\begin{aligned} L_f[f_q(\xi) - \chi_q f_{q-1}(\xi)] &= \hbar_f U_q^f(\xi), \quad g_g[g_q(\xi) - \chi_q g_{q-1}(\xi)] = \hbar_g U_q^g(\xi), \\ L_\theta[\theta_q(\xi) - \chi_q \theta_{q-1}(\xi)] &= \hbar_\theta U_q^\theta(\xi), \quad L_\Phi[\Phi_q(\xi) - \chi_q \Phi_{q-1}(\xi)] = \hbar_\Phi U_q^\Phi(\xi). \end{aligned} \tag{32}$$

The equivalent boundary conditions are:

$$\begin{aligned} f_q(0) &= f'_q(0) = f'_q(\infty) = 0, \\ g_q(0) &= g'_q(0) = g'_q(\infty) = 0, \\ \theta'_q(0) &= \theta_q(\infty) = 0 \\ \Phi_q(0) &= \Phi_q(\infty) = 0, \end{aligned} \tag{33}$$

Here

$$U_q^f(\xi) = f'''_{q-1} - 2 \sum_{k=0}^{q-1} (f'_{q-1} + g'_{q-1}) f'_k + \sum_{k=0}^{q-1} (f_{q-1} + g_{q-1}) f''_k - K \sum_{k=0}^{q-1} f_{q-1}^v - \sum_{k=0}^{q-1} \{(M^2 + \kappa + Fr f'_{q-1}) f'_k\}, \tag{34}$$

$$U_q^g(\xi) = g'''_{q-1} - 2 \sum_{k=0}^{q-1} (f'_{q-1} + g'_{q-1}) g'_k + \sum_{k=0}^{q-1} (f_{q-1} + g_{q-1}) g''_k - K \sum_{k=0}^{q-1} g_{q-1}^v - \sum_{k=0}^{q-1} \{(M^2 + \kappa + Fr g'_{q-1}) g'_k\}, \tag{35}$$

$$\begin{aligned} U_q^\theta(\xi) &= \frac{1}{Pr} \theta''_{q-1} - A \sum_{k=0}^{q-1} (f'_{q-1} + g'_{q-1}) \theta_k + \sum_{k=0}^{q-1} (f_{q-1} + g_{q-1}) \theta'_k \\ &+ \frac{A}{2} \left[\left\{ \xi \sum_{k=0}^{q-1} (f'_{q-1} + g'_{q-1}) + (1 + 2A) \sum_{k=0}^{q-1} (f_{q-1} + g_{q-1}) \right\} \sum_{k=0}^{q-1} (f'_{q-1} + g'_{q-1}) \theta'_k \right. \\ &\left. - A \left[(A + 2) \sum_{k=0}^{q-1} (f'_{q-1} + g'_{q-1})^2 + \sum_{k=0}^{q-1} (f_{q-1} + g_{q-1}) (f''_{q-1} + g''_{q-1}) \right] \theta_k - \sum_{k=0}^{q-1} (f_{q-1} + g_{q-1})^2 \theta''_k \right] \end{aligned} \tag{36}$$

$$U_q^\Phi(\xi) = \Phi''_{q-1} - ScA \sum_{k=0}^{q-1} (f'_{q-1} + g'_{q-1}) \Phi_k + Sc \sum_{k=0}^{q-1} (f_{q-1} + g_{q-1}) \Phi'_k + \frac{Nt}{Nb} \theta''_{q-1}, \tag{37}$$

where

$$\chi_q = \begin{cases} 0, & \text{if } \Re \leq 1 \\ 1, & \text{if } \Re > 1 \end{cases}. \tag{38}$$

4. HAM Convergence

The velocity profiles convergence, temperature profile convergence, and concentration profile convergence are obtained through supporting parameters $\hbar_f, \hbar_g, \hbar_\theta$, and \hbar_Φ of HAM are presented in Figures 2 and 3. These legal \hbar -curves show the convergence regions for HAM.

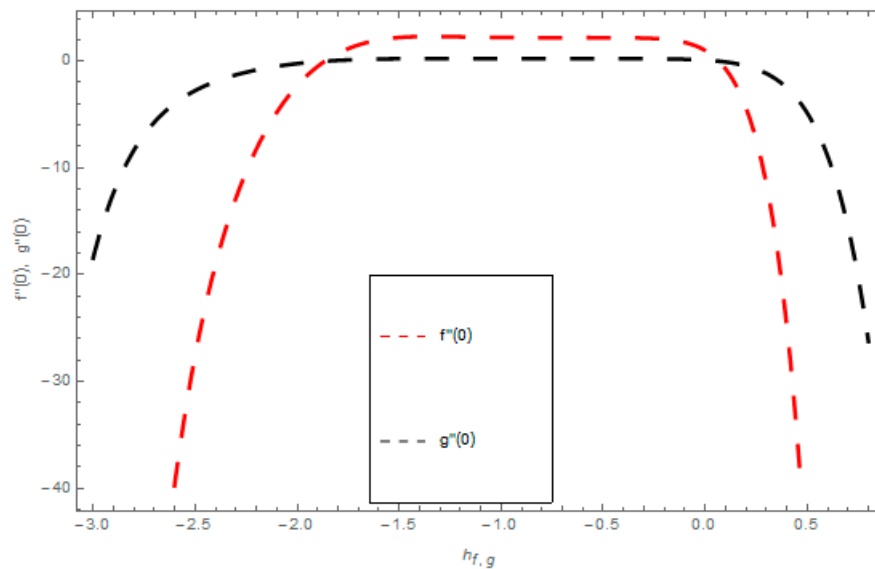


Figure 2. The h -curves graph for velocity fields.

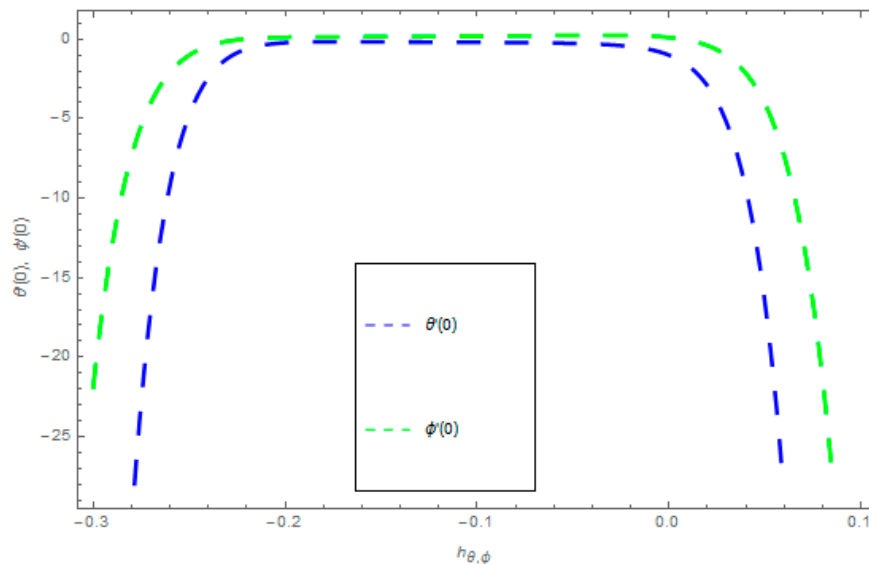


Figure 3. The h -curves graph for temperature and concentration fields.

5. Results and Discussion

This section describes the impacts of dimensionless parameters that arose while studying the fluids flow phenomena. These parameters are magnetic field parameter, M , ratio of rates parameter, α , porosity parameter, κ , coefficient of inertia, Fr , couple stress parameter, K , thermal relaxation time, Λ , Brownian motion parameter, Nb , Schmidt number, Sc , and thermophoresis parameter, Nt . The impression of M on $f'(\xi)$ and $g'(\xi)$ is demonstrated in Figure 4. Theory of Lorentz force tells us that escalating M decreases $f'(\xi)$ and $g'(\xi)$. Large values of magnetic field M produce more collisions among molecules, which yield the opposite force to the flow. Therefore, the behavior of fluid flow falls down. The impression of κ on $f'(\xi)$ and $g'(\xi)$ is demonstrated through Figure 5. The porous media plays a significant role in the fluid flow phenomena. The porous media increases the opposing force to fluid flow, which reduces the motion of fluid particles and subsequently the velocity of the fluid reduces. An analogous effect of κ on $g'(\xi)$ is depicted here. The impression of Fr on $f'(\xi)$ and $g'(\xi)$ is revealed in Figure 6. Fr has an inverse relationship with the fluid flow. The increasing Fr reduces the fluid flow motion. This impact is due to the direct relationship of the coefficient of inertia and porous

media. As mentioned above, the fluid flow motion reduces in the porous media. The impression of α on $f'(\xi)$ and $g'(\xi)$ is displayed in Figure 7. Large values of α upsurges $f'(\xi)$, but declines $g'(\xi)$. This effect is due to more dominance in α along the y-direction of the fluid flow, as compared to α in the x-direction. The impression of K on $f'(\xi)$ and $g'(\xi)$ is demonstrated in Figure 8. K is directly proportional to couple stress viscosity parameter n . Larger numerical values of K provides more viscosity of the fluid, which reduces fluid flow and, as a result, reduction in $f'(\xi)$ and $g'(\xi)$ is obtained. The influence of Λ on $\theta(\xi)$ is demonstrated through Figure 9. Here, it is noticed that there is an inverse relationship between Λ and $\theta(\xi)$. The increasing values of Λ reduces the temperature of the fluid flow. Additionally, Λ versus A is studied. The negative A has an inverse relationship with Λ , while the positive A has a direct relationship with Λ . Thus, the negative A has a dominant impact on the fluid flow. The thermal relaxation time refers to a classical Fourier's law of conduction. So, it is realized that if temperature is very low than a classical Fourier's conduction model is obtained. Impact of Pr on $\theta(\xi)$ is displayed in Figure 10. Here it is observed that higher numerical values of Pr declines $\theta(\xi)$. We deduce from this effect that small numerical values of Pr causes high thermal conductivity, while this effect is quite opposite for large numerical values of Pr . It is important to discuss the impact of A on Pr . The positive A is more effective on Pr as compared to negative A . In addition, negative A plays a dominant role in Pr . The impact of A on $\theta(\xi)$ is shown in Figure 11. A and $\theta(\xi)$ have an inverse relationship. The escalating A reduces $\theta(\xi)$. It is interesting to mention that the positive values of A plays a dominant role in temperature distribution of the fluid flow, as compared to negative values of A . The effect of Nb on $\phi(\xi)$ is demonstrated through Figure 12. The higher values of Nb boosts the motion of nanoparticles inside the fluid, which results in a reduction of fluid concentration. Thus, large numerical values of Nb reduces $\phi(\xi)$. It is interesting to mention that the negative values of A plays a dominant role in Brownian motion. The impact of Nt on $\phi(\xi)$ is portrayed through Figure 13. Large values of Nt increases $\phi(\xi)$. This is because of the fact that larger values of Nt thrust the nanoparticles of the fluid from the hot region, which results in the increase of $\phi(\xi)$. It is interesting to mention that the negative A plays a dominant role in Nt . Impact of Sc on $\phi(\xi)$ is portrayed in Figure 14. Really, the weak diffusivity of mass is noted for higher Sc values. This weak diffusivity of mass has a marvelous effect on fluid concentration, which results in the decrease of $\phi(\xi)$. Here, in the Schmidt number, the positive A plays a dominant role. The impact of A on $\phi(\xi)$ is depicted in Figure 15. Here we have an interesting behavior of A . Both the positive and negative A have an increasing behavior in $\phi(\xi)$. But the negative A is more dominant on concentration as compared to positive A .

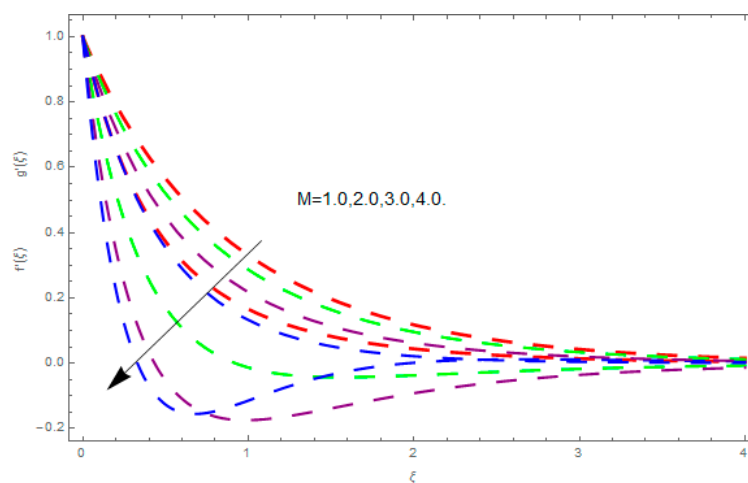


Figure 4. Impression of M on $f'(\xi)$ and $g'(\xi)$.

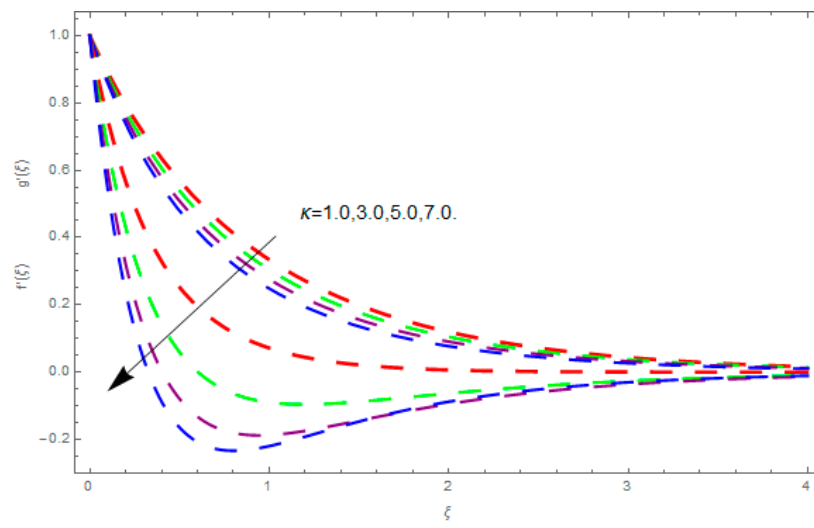


Figure 5. Impression of κ on $f'(\xi)$ and $g'(\xi)$.

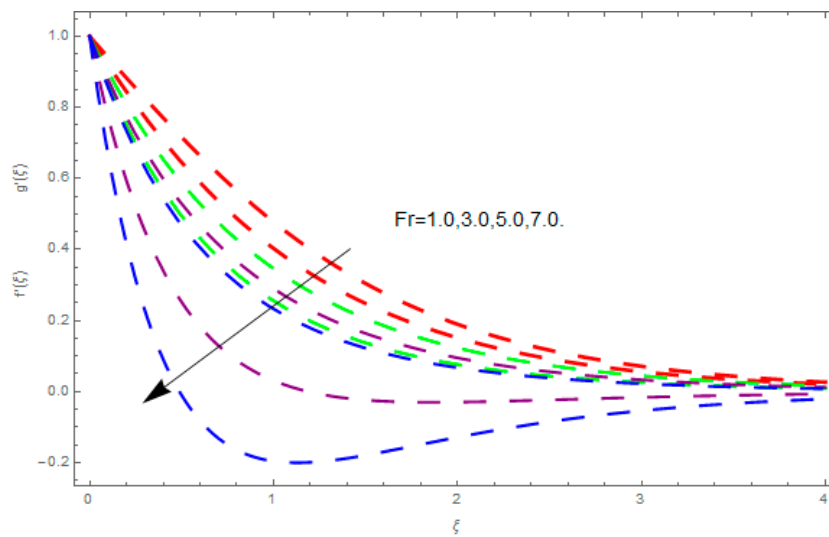


Figure 6. Impression of Fr on $f'(\xi)$ and $g'(\xi)$.

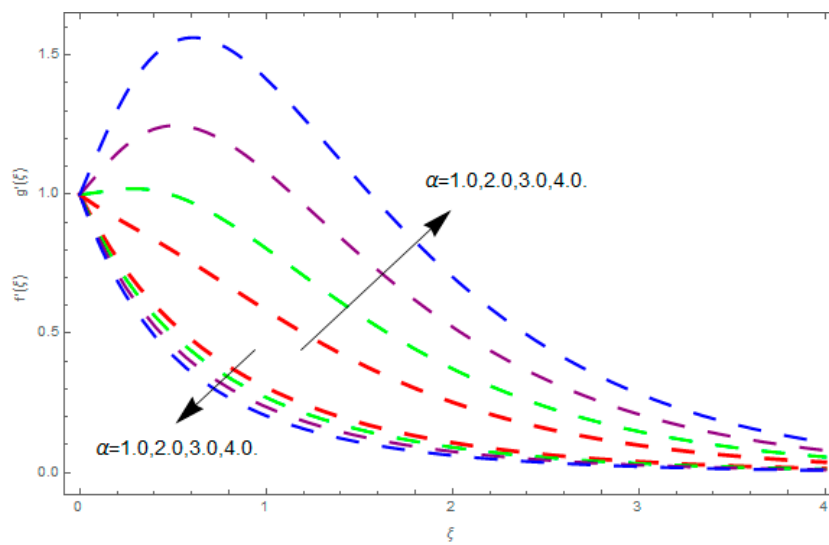


Figure 7. Impression of α on $f'(\xi)$ and $g'(\xi)$.

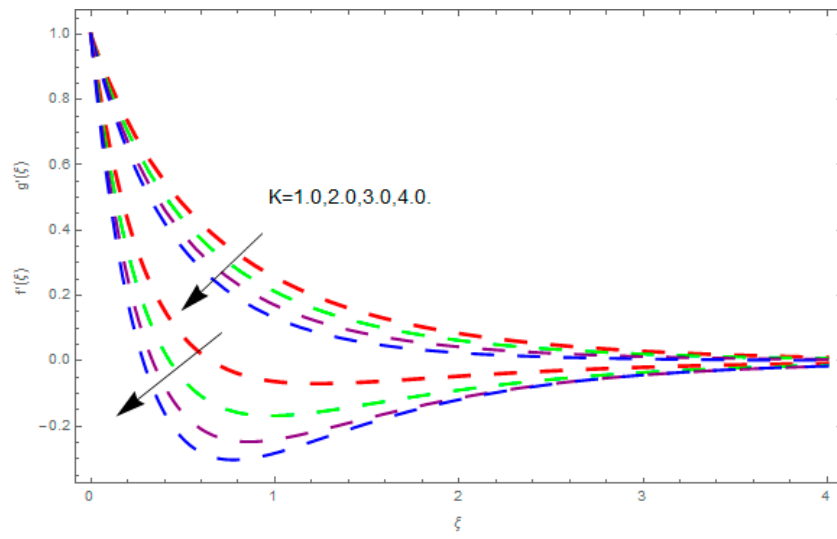


Figure 8. Impression of K on $f'(\xi)$ and $g'(\xi)$.

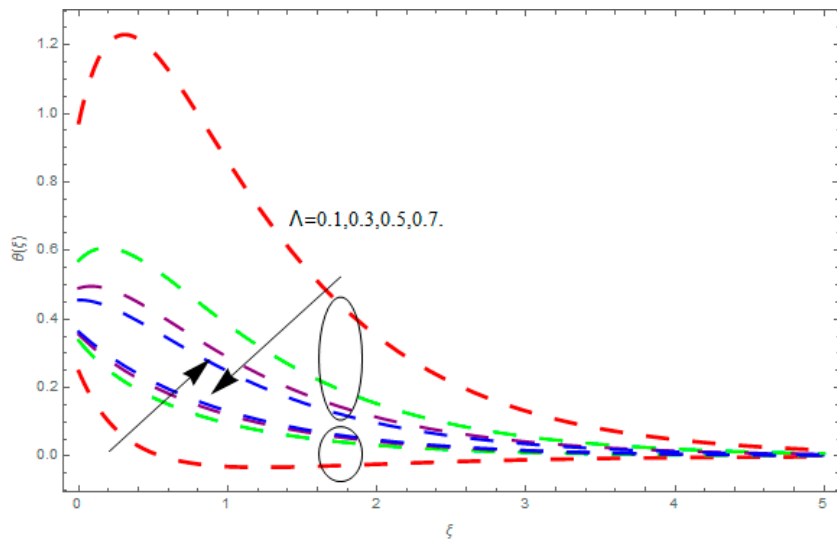


Figure 9. Impression of Λ on $\theta(\xi)$.

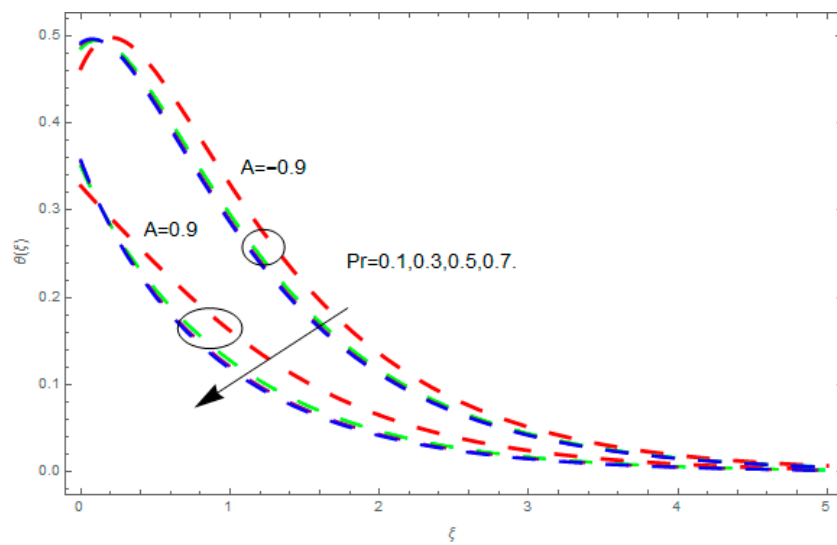


Figure 10. Impression of Pr on $\theta(\xi)$.

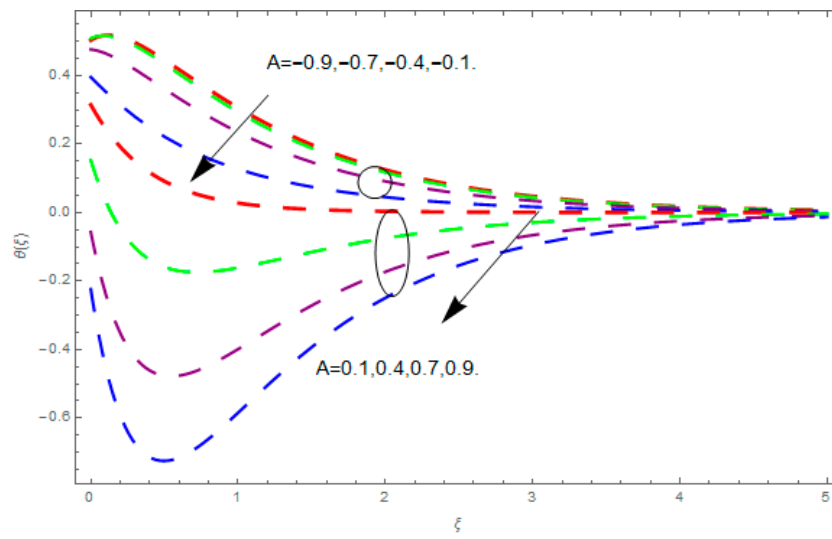


Figure 11. Impression of A on $\theta(\xi)$.

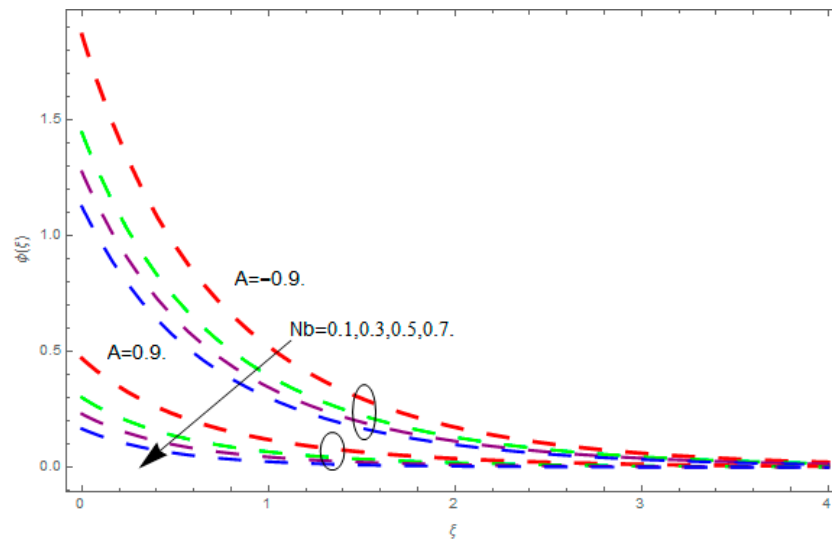


Figure 12. Impression of Nb on $\phi(\xi)$.

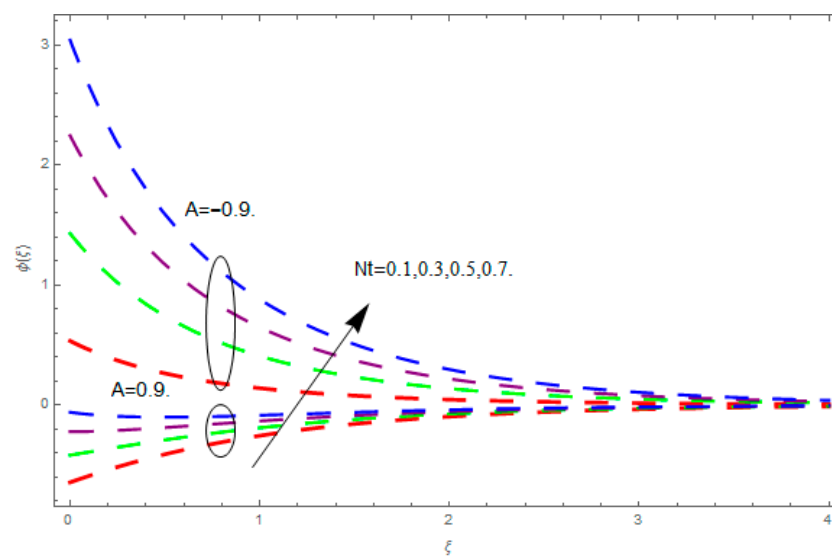


Figure 13. Impression of Nt on $\phi(\xi)$.

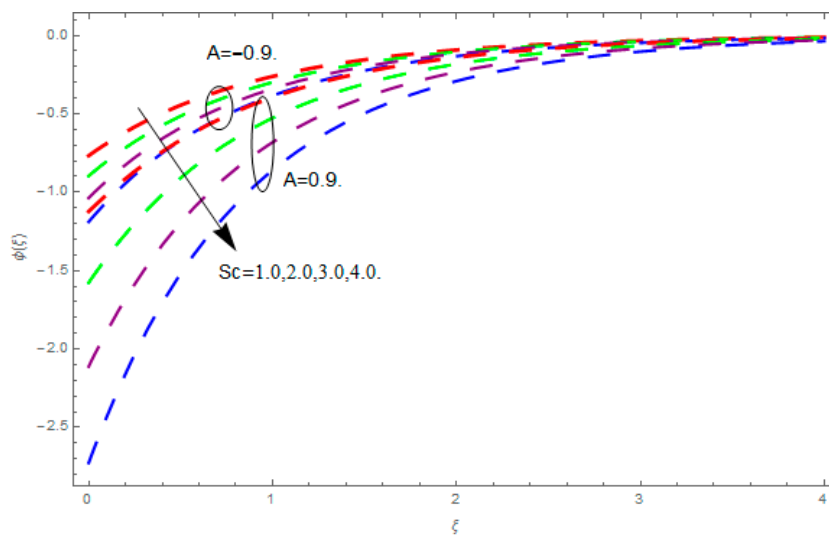


Figure 14. Impression of Sc on $\phi(\xi)$.

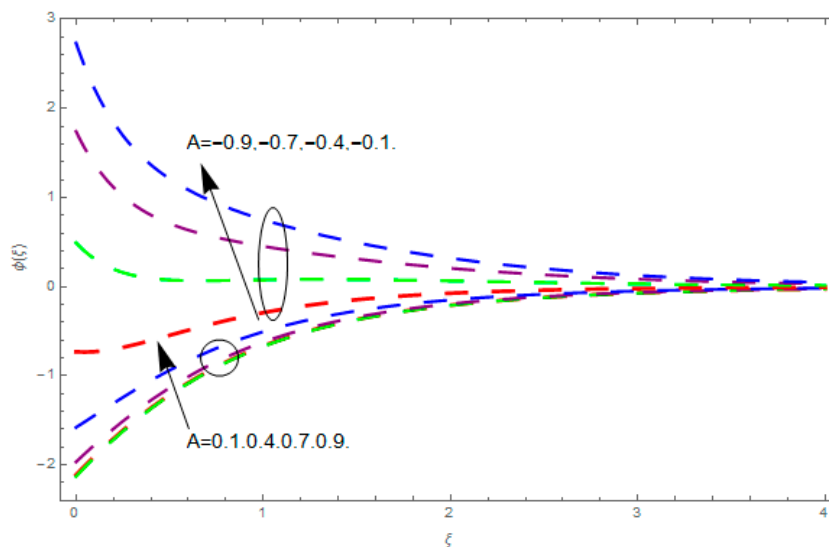


Figure 15. Impression of A on $\phi(\xi)$.

6. Tables Discussion

Tables 1 and 2 demonstrate the outcomes of incipient parameters on skin friction coefficients in x - and y -directions, respectively. Parameters under discussion are ratio of rates parameter, α , couple stress, K , magnetic field, M , porosity, κ , and coefficient of inertia, Fr . We observed that higher ratio of rates, α , couple stress, K , magnetic field, M , and porosity, κ , boost the skin friction coefficient, while higher values of inertia, Fr , falloff the skin friction coefficient. The results were compared with Ramzan et al. [21] and showed a very close agreement.

Table 1. Calculation of skin friction coefficient $C_f Re_x^{1/2}$ for $\alpha, K, M, Fr,$ and κ .

α	K	M	Fr	κ	Ramzan et al. [21]	Present Study
0.1					1.43588	1.435881
0.2					1.45336	1.453367
0.3					1.51480	1.514801
0.1	0.02				1.48241	1.482410
	0.03				1.58900	1.589002
	0.01	0.1			1.37723	1.377231
		0.2			1.38939	1.389390
		0.3			1.40891	1.408911
		0.1	0.2		-	1.268100
			0.3		-	1.265650
			0.4		-	1.263190
			0.1	0.1	-	1.273000
				0.2	-	1.275451
				0.3	-	1.277892

Table 2. Calculation of skin friction coefficient $C_g Re_x^{1/2}$ for $\alpha, K, M, Fr,$ and κ .

α	K	M	Fr	κ	Ramzan et al. [21]	Current Study
0.1					0.143578	0.143577
0.2					0.299583	0.299582
0.3					0.467421	0.467420
0.4					0.646402	0.646401
0.1	0.02				0.147835	0.147834
	0.03				0.154193	0.154192
	0.04				0.164693	0.164692
	0.01	0.5			0.146938	0.146937
		0.6			0.150971	0.150970
		0.7			0.155608	0.155607
			0.2		-	0.331610
			0.3		-	0.330969
			0.4		-	0.330280
				0.1	-	0.330966
				0.2	-	0.331603
				0.3	-	0.332237

7. Conclusions

The 3D magnetohydrodynamics flow of Darcy–Forchheimer couple stress nanofluid flow over an exponentially stretching sheet is presented. To examine the relaxation characteristics, the proposed model of Cattaneo–Christov is applied. For the first time, the influence of the temperature exponent is explored in the current work.

The concluding remarks are given as:

- The augmented ratio of rates parameter increases the velocity profile in the x-direction.
- The augmented magnetic field, porosity parameter, coefficient of inertia, and couple stress parameter diminishes the velocity field along the x– direction.
- The augmented magnetic field, porosity parameter, coefficient of inertia, ratio of rates parameter, and couple stress parameter reduces the velocity field along the y– axis.
- The enhancement in Prandtl number, time relaxation, and temperature exponent reduces the temperature field.
- The augmented thermophoresis and temperature exponent upsurges the concentration field.
- The augmented Brownian motion and Schmidt number reduces the concentration field.

- The augmented ratio of rates, couple stress, magnetic field, and porosity parameters upsurges the skin friction coefficient.
- The augmented coefficient of inertia diminishes the skin friction coefficient.

Author Contributions: M.W.A., Z.S. and R.N.: Conceptualization; methodology; software; validation; writing—original draft preparation; writing—review and editing. A.A.F., A.D and S.I.: Conceptualization; methodology; software; visualization; writing—review and editing. P.K. and P.T.: Writing—review and editing; visualization; project administration; funding acquisition; investigation; resources.

Funding: This research was funded by the Center of Excellence in Theoretical and Computational Science (TaCS-CoE), KMUTT.

Acknowledgments: This project was supported by the Theoretical and Computational Science (TaCS) Center under Computational and Applied Science for Smart Innovation Research Cluster (CLASSIC), Faculty of Science, KMUTT.

Conflicts of Interest: The authors declare that they have no competing interests.

Nomenclature

A	Temperature exponent
U_0, V_0	Constants
0	Magnetic field strength (NmA^{-1})
C	Coefficient of concentration
C_f	Skin friction coefficient
c_p	Specific heat ($\text{Jkg}^{-1}\text{K}^{-1}$)
D_B	Brownian diffusion of nanofluids
D_T	Thermophoretic diffusion of nanofluids
E	Electric field (NC^{-1})
f, g	Dimensional velocity profiles
K	Couple stress parameter
L	Reference length (m)
M	Hartmann number
Nb	Brownian motion
Nt	Thermophoretic parameter
u_x	Nusselt number
Pr	Prandtl number
q_r	Heat flux (Wm^{-2})
Re_x	Local Reynolds number
Sc	Schmidt number
Sh_x	Sherwood number
T	Fluid temperature (K)
u, v, w	Velocity components (ms^{-1})
x, y, z	Coordinates
$y_i (i = 1 - 10)$	Constants

Greek Letters

α	Ratio of rates parameter
Λ	Thermal relaxation time
γ	Biot number
θ	Dimensional heat profile
Φ	Dimensional concentration profile
ξ	Similarity variable
ν	Kinematic viscosity (m^2s^{-1})
κ	Porosity parameter
ρ	Fluid density (Kgm^{-3})
σ_{nf}	Electrical conductivity (Sm^{-1})

References

1. Choi, S.U.S.; Eastman, J.A. Enhancing thermal conductivity of fluids with nanoparticles. *ASME Publ. Fed.* **1995**, *231*, 99–106.
2. Wang, X.Q.; Mujumdar, A.S. Heat transfer characteristics of nanofluids: A review. *Int. J. Therm. Sci.* **2007**, *46*, 1–19. [[CrossRef](#)]
3. Eastman, J.A.; Phillpot, S.R.; Choi, S.U.S.; Keblinski, P. Thermal transport in nanofluids. *Annu. Rev. Mater. Res.* **2004**, *34*, 219–246. [[CrossRef](#)]
4. Eastman, J.A.; Choi, S.U.S.; Li, S.; Yu, W.; Thompson, L.J. Anomalous increased effective thermal conductivities of ethylene glycol-based nanofluids containing copper nanoparticles. *Appl. Phys. Lett.* **2001**, *78*, 718–720. [[CrossRef](#)]
5. Tiwari, R.K.; Das, M.K. Heat transfer augmentation in a two-sided lid-driven differentially heated square cavity utilizing nanofluids. *Int. J. Heat Mass Transf.* **2007**, *50*, 2002–2018. [[CrossRef](#)]
6. Buongiorno, J. Convective transport in nanofluids. *J. Heat Transf.* **2006**, *128*, 240–250. [[CrossRef](#)]
7. Kasaeian, A.; Daneshzarian, R.; Mahian, O.; Chamkha, A.J.; Wingwises, S.; Pop, I. Nanofluid flow and heat transfer in porous media: A review of the latest developments. *Int. J. Heat Mass Transf.* **2017**, *107*, 778–791. [[CrossRef](#)]
8. Ramzan, M.; Chung, J.D.; Ullah, N. Radiative magnetohydrodynamic nanofluid flow due to gyrotactic microorganisms with chemical reaction and non-linear thermal radiation. *Int. J. Mech. Sci.* **2017**, *130*, 31–40. [[CrossRef](#)]
9. Sheikholeslami, M.; Shah, Z.; Shafi, A.; Khan, I.; Itili, I. Uniform magnetic force impact on water based nanofluid thermal behavior in a porous enclosure with ellipse shaped obstacle. *Sci. Rep.* **2019**, *9*, 1196. [[CrossRef](#)]
10. Besthapu, P.; Haq, R.U.; Bandari, S.; Al-Mdallal, Q.M. Mixed convection flow of thermally stratified MHD nanofluid over an exponentially stretching surface with viscous dissipation effect. *J. Taiwan Inst. Chem. E* **2017**, *71*, 307–314. [[CrossRef](#)]
11. Dawar, A.; Shah, Z.; Idrees, M.; Khan, W.; Islam, S.; Gul, T. Impact of thermal radiation and heat source/sink on eyring–powell fluid flow over an unsteady oscillatory porous stretching surface. *Math. Comput. Appl.* **2018**, *23*, 20. [[CrossRef](#)]
12. Alharbi, S.O.; Dawar, A.; Shah, Z.; Khan, W.; Idrees, M.; Islam, S.; Khan, I. Entropy generation in MHD eyring–powell fluid flow over an unsteady oscillatory porous stretching surface under the impact of thermal radiation and heat source/sink. *Appl. Sci.* **2018**, *8*, 2588. [[CrossRef](#)]
13. Shah, Z.; Dawar, A.; Islam, S.; Khan, I.; Ching, D.L.C. Darcy-Forchheimer flow of radiative carbon nanotubes with microstructure and inertial characteristics in the rotating frame. *Stud. Therm. Eng.* **2018**, *12*, 823–832. [[CrossRef](#)]
14. Khan, A.; Shah, Z.; Islam, S.; Dawar, A.; Bonyah, E.; Ullah, H.; Khan, A. Darcy-Forchheimer flow of MHD CNTs nanofluid radiative thermal behaviour and convective non uniform heat source/sink in the rotating frame with microstructure and inertial characteristics. *AIP Adv.* **2018**, *8*, 125024. [[CrossRef](#)]
15. Zubair, M.; Shah, Z.; Islam, S.; Khan, W.; Dawar, A. 3D Darcy-Forchhemier squeezing nanofluid flow with Cattaneo-Christov heat flux through porous medium in spinning coordinates. *Adv. Mech. Eng.* **2019**, *11*, 1–17. [[CrossRef](#)]
16. Khan, A.S.; Nie, Y.; Shah, Z.; Dawar, A.; Khan, W.; Islam, S. Three-dimensional nanofluid flow with heat and mass transfer analysis over a linear stretching surface with convective boundary conditions. *Appl. Sci.* **2018**, *8*, 2244. [[CrossRef](#)]
17. Dawar, A.; Shah, Z.; Khan, W.; Idrees, M.; Islam, S. Unsteady squeezing flow of magnetohydrodynamic carbon nanotube nanofluid in rotating channels with entropy generation and viscous dissipation. *Adv. Mech. Eng.* **2019**, *11*, 1–18. [[CrossRef](#)]
18. Sheikholeslami, M. Numerical investigation of nanofluid free convection under the influence of electric field in a porous enclosure. *J. Mol. Liq.* **2018**, *249*, 1212–1221. [[CrossRef](#)]
19. Sheikholeslami, M. CuO-water nanofluid flow due to magnetic field inside a porous media considering Brownian motion. *J. Mol. Liq.* **2018**, *249*, 921–929. [[CrossRef](#)]

20. Dawar, A.; Shah, Z.; Khan, W.; Islam, S.; Idrees, M. An optimal analysis for Darcy-Forchheimer 3-D Williamson Nanofluid Flow over a stretching surface with convective conditions. *Adv. Mech. Eng.* **2019**, *11*, 1–15. [[CrossRef](#)]
21. Ramzan, M.; Sheikholeslami, M.; Saeed, M.; Chung, J.D. On the convective heat and zero nanoparticle mass flux conditions in the flow of 3D MHD Couple Stress nanofluid over an exponentially stretched surface. *Sci. Rep.* **2019**, *9*, 562. [[CrossRef](#)]
22. Fourier, J.B.J. *Théorie Analytique De La Chaleur*; Didot: Paris, France, 1822.
23. Cattaneo, C. Sulla conduzione del calore. *Atti Sem. Mat. Fis. Univ. Modena* **1948**, *3*, 83–101.
24. Christov, C.I. On frame indifferent formulation of the Maxwell-Cattaneo model of finite-speed heat conduction. *Mech. Res. Commun.* **2009**, *36*, 481–486. [[CrossRef](#)]
25. Straughan, B. *Stability and Wave Motion in Porous Media*; Springer: New York, NY, USA, 2008; Volume 165.
26. Straughan, B. Thermal convection with the Cattaneo-Christov model. *Int. J. Heat Mass Transf.* **2010**, *53*, 95–98. [[CrossRef](#)]
27. Han, S.; Zheng, L.; Li, C.; Zhang, X. Coupled flow, and heat transfer in viscoelastic fluid with Cattaneo-Christov heat flux model. *Appl. Math. Lett.* **2014**, *38*, 87–93. [[CrossRef](#)]
28. Khan, J.A.; Mustafa, M.; Hayat, T.; Alsaedi, A. Numerical study of Cattaneo-Christov heat flux model for viscoelastic flow due to an exponentially stretching surface. *PLoS ONE* **2015**, *10*, e0137363.
29. Hayat, T.; Nadeem, S. Aspects of developed heat and mass flux models on 3D flow of Eyring-Powell fluid. *Results Phys.* **2017**, *7*, 3910–3917. [[CrossRef](#)]
30. Tibullo, V.; Zampoli, V. A uniqueness result for the Cattaneo-Christov heat conduction model applied to incompressible fluids. *Mech. Res. Commun.* **2011**, *38*, 77–79. [[CrossRef](#)]
31. Ciarletta, M.; Straughan, B. Uniqueness and structural stability for the Cattaneo-Christov equations. *Mech. Res. Commun.* **2010**, *37*, 445–447. [[CrossRef](#)]
32. Haddad, S.A.M. Thermal instability in Brinkman porous media with Cattaneo-Christov heat flux. *Int. J. Heat Mass Transf.* **2014**, *68*, 659–668. [[CrossRef](#)]
33. Mustafa, M. Cattaneo-Christov heat flux model for rotating flow and heat transfer of upper-convected Maxwell fluid. *AIP Adv.* **2015**, *5*, 047109. [[CrossRef](#)]
34. Hayat, T.; Farooq, M.; Alsaedi, A.; Al-Solamy, F. Impact of Cattaneo-Christov heat flux in the flow over a stretching sheet with variable thickness. *AIP Adv.* **2015**, *5*, 087159. [[CrossRef](#)]
35. Waqas, M.; Hayat, T.; Farooq, M.; Shehzad, S.A.; Alsaedi, A. Cattaneo-Christov heat flux model for flow of variable thermal conductivity generalized Burgers fluid. *J. Mol. Liq.* **2016**, *220*, 642–648. [[CrossRef](#)]
36. Li, J.; Zheng, L.; Liu, L. MHD viscoelastic flow and heat transfer over a vertical stretching with Cattaneo-Christov heat flux. *J. Mol. Liq.* **2016**, *221*, 19–25. [[CrossRef](#)]
37. Shah, Z.; Dawar, A.; Khan, I.; Islam, S.; Ching, D.L.C.; Khan, A.Z. Cattaneo-Christov model for electrical magnetite micropolar Casson ferrofluid over a stretching/shrinking sheet using effective thermal conductivity model. *Case Stud. Therm. Eng.* **2019**, *13*, 100352. [[CrossRef](#)]
38. Hayat, T.; Nadeem, S. Flow of 3D Eyring-Powell fluid by utilizing Cattaneo-Christov heat flux model and chemical processes over an exponentially stretching surface. *Results Phys.* **2018**, *8*, 397–403. [[CrossRef](#)]
39. Muskat, M. *The Flow of Homogeneous Fluids through Porous Media*; Edwards: Ann Arbor, MI, USA, 1946.
40. Seddeek, M.A. Influence of viscous dissipation and thermophoresis on Darcy-Forchheimer mixed convection in a fluid saturated porous media. *J. Colloid Interface Sci.* **2006**, *293*, 137–142. [[CrossRef](#)]
41. Pal, D.; Mondal, H. Hydromagnetic convective diffusion of species in Darcy-Forchheimer porous medium with non-uniform heat source/sink and variable viscosity. *Int. Commun. Heat Mass Transf.* **2012**, *39*, 913–917. [[CrossRef](#)]
42. Sadiq, M.A.; Hayat, T. Darcy-Forchheimer flow of magneto Maxwell liquid bounded by convectively heated sheet. *Results Phys.* **2016**, *6*, 884–890. [[CrossRef](#)]
43. Abderrahim, W.; Zoubair, B.; Rachid, S. Numerical analysis of the onset of longitudinal convective rolls in a porous medium saturated by an electrically conducting nanofluid in the presence of an external magnetic field. *Results Phys.* **2017**, *7*, 2134–2152.
44. Wakif, A.; Boulahia, Z.; Ali, F.; Mohamed, R.E.; Rachid, S. Numerical Analysis of the Unsteady Natural Convection MHD Couette Nanofluid Flow in the Presence of Thermal Radiation Using Single and Two-Phase Nanofluid Models for Cu-Water Nano fluids. *Int. J. Appl. Comput. Math.* **2018**, *4*, 81. [[CrossRef](#)]

45. Wakif, A.; Boulahia, Z.; Mishra, S.R.; Rashidi, M.M.; Sehaqui, R. Influence of a uniform transverse magnetic field on the thermo-hydrodynamic stability in water-based nanofluids with metallic nanoparticles using the generalized Buongiorno's mathematical model. *Eur. Phys. J. Plus* **2018**, *133*, 181. [[CrossRef](#)]
46. Abderrahim, W.; Zoubair, B.; Rachid, S. Numerical Study of the Onset of Convection in a Newtonian Nanofluid Layer with Spatially Uniform and Non Uniform Internal Heating. *J. Nanofluids* **2017**, *6*, 136–148.
47. Abderrahim, W.; Zoubair, B.; Rachid, S. A semi-analytical analysis of electro-thermo hydrodynamic stability in dielectric nanofluids using Buongiorno's mathematical model together with more realistic boundary conditions. *Results Phys.* **2018**, *9*, 1438–1454.
48. Wakif, A.; Boulahia, Z.; Amine, A.; Animasaun, I.L.; Afridi, M.I.; Qasim, M.; Sehaqui, R. Magneto-convection of alumina-water nanofluid within thin horizontal layers using the reccised generalized Buongiorno's model. *Front. Heat Mass Transf. (FHMT)* **2019**, *12*, 3.
49. Wakif, A.; Qasim, M.; Afridi, M.; Saleem, S.; Al-Qarni, M.M. Numerical examination of the entropic energy harvesting in a magnetohydrodynamic dissipative flow of stokes' second problem: utilization of the gear-generalized differential quadrature method. *J. Non-Equilib. Thermodyn.* **2019**. [[CrossRef](#)]
50. Zubair, M.; Shah, Z.; Dawar, A.; Islam, S.; Kumam, P.; Khan, A. Entropy generation optimization in squeezing magnetohydrodynamics flow of casson nanofluid with viscous dissipation and joule heating effect. *Entropy* **2019**, *21*, 747. [[CrossRef](#)]



© 2019 by the authors. Licensee MDPI, Basel, Switzerland. This article is an open access article distributed under the terms and conditions of the Creative Commons Attribution (CC BY) license (<http://creativecommons.org/licenses/by/4.0/>).